Multicomponent Self-assembly of a Multinuclear Heterometal–Organic Polymer for CO2 Reduction

Ke Qiao

MOE Key Laboratory of Cluster Science, Beijing Key Laboratory of Photoelectronic/Electrophotonic Conversion Materials, School of Chemistry and Chemical Engineering, Beijing Institute of Technology, Beijing, P. R. China

3120211220@bit.edu.cn

Abstract. To address the greenhouse effect, scientists have never stopped exploring efficient photocatalytic CO2 reduction systems, and metal-organic compounds have recently emerged as a solution for overcoming global warming and climate issues. Under the irradiation of visible light, the catalytic activity, stability, and selectivity of most of the non-noble metal complexes reported so far are unsatisfactory. To efficiently fix CO2, Ru multinuclear heterometal–organic compound was obtained for carbon dioxide reduction. The as-synthesized M-Zn complex (M =Ru) catalysts exhibit special catalytic activity for the reduction of CO2 because of the immobilized metal ions serving as active sites during the reaction. This study proposes a general strategy for CO2 reduction through high levels in metal-organic polymers to achieve effective environmental protection and governance.

Keywords: Cooperative effects, Nanoparticles, Functional, Carbon dioxide reduction.

1. Introduction

Excessive carbon dioxide emissions are considered to be one of the main causes of global climate change. Therefore, it has attracted widespread attention. [1–3] By mimicking the natural photosynthesis process, artificial photosynthesis for photocatalytic conversion of CO_2 and high value-added carbon products such as CO driven by solar lamps will be a promising strategy to accelerate the carbon cycle and solve the problem of excessive carbon dioxide in the world.[4-6] Therefore, researchers have been working to find photocatalysts that can efficiently reduce CO_2 to CO. Capturing and converting CO_2 into CO fuel has become one of the hotspots of scientific research due to its advantages in solving solutions that solve both carbon emissions and energy crises. [7–13]

Various compounds have been explored for stereochemical reactions.[14-18] The main approach is to utilize metal-organic compounds with restricted shapes and sizes to control the chemo-, regio-, and stereoselectivity of a certain transformation.[19-24] Some of the metal-organic compounds involve homoleptic metallic unit centers featuring specific coordination geometry. Carbon sequestration is a process through which atmospheric freely available carbon dioxide (CO_2) is captured and stored through a natural process, so it has become a most important feature in environmental protection. For better results, the material should be of large surface area for effective absorption and easy accessibility to atmospheric carbon dioxide.[25] Therefore, it is important to capture CO_2 from the environment to make the environment clean.

Heterogeneous catalysts generally have good processability and recyclability. When metal complexes are immobilized on a solid matrix, the dissociation of the ligand from the center of the metal atom may be inhibited due to mobility limitations, which should result in a longer service life. [26,27] Here we report a partially heterogeneous CO_2 photoreduction system, where Ir(III) and Zn(II) were fixed to a polymer and it was added in a mixture of dimethylformamide (DMA) as the solvent and tri-ethanol amine (TEOA) as a reducing agent and the amount of produced CO was discussed.

Herein, we report a novel metal-organic polymer Ir-Zn containing Ir(III) and Zn(II) centers by subcomponent self-assembly (Scheme 1) for the reduction of carbon dioxide. In this work, the obtained compounds display excellent catalytic performance in a series of liquid-phase reactions owing to a decrease in the diffusion resistance from the substrate to the product immobilized by the metal-organic polymer support. Photocatalytic CO_2 reduction was performed in a partially heterogeneous system using Ir and Zn complexes: Ir(III) as a photosensitizer was fixed to cation exchange polymers while Zn(II) was used as a catalyst. Experiments were also conducted on the reuse of complexes in homogeneous systems, the results show that the complex can be reused after replacing the original gas with new CO_2.

2. Experimental

2.1 Materials

Unless stated otherwise, all chemicals were of reagent grade quality obtained from commercial sources and used without further purification. All reactions were carried out under a nitrogen atmosphere, unless stated otherwise. Abbreviations:ppy = 2-(3-Nitrophenyl)pyridine; nm = nanometres; min = minute(s); h = hour(s); rt = room temperature (20 °C).

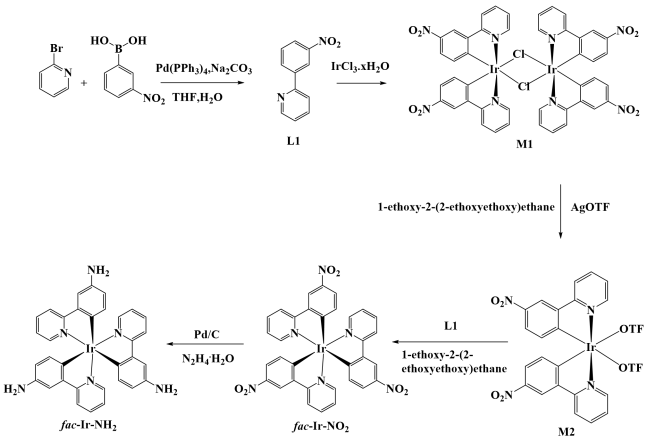

Scheme 1. Synthesis of *fac*-Ir-NH_2.

2.2 Characterizations

Fourier transforms infrared (FT-IR) spectra were recorded in transmission mode on a Smart Omni-Transmission spectrometer using KBr pellets in the range 400-4000cm^{-1}. The powder X-ray diffraction (XRD) patterns of the products were measured using Bruker D8 Advance. The morphology analysis was carried out by Hitachi S-4800 scanning electron microscopy (SEM, Japan).

2.2.1 Synthesis of [Ir(ppy)2(μ-Cl)]2 (M1)

$IrCl_3 \cdot xH_2O$ (0.35 g, 1 mmol) was refluxed with 2.2 equiv of cyclometalating ligand L_1(0.44 g, 2.2 mmol) in a 3:1 mixture of 1-ethoxy-2-(2-ethoxyethoxy) ethane and water, and the reaction mixture was stirred for 48 h at 120 °C. The reaction mixture was filtered, washed with water and tetrahydrofuran. The yellow solids were collected and dried under vacuum to give the product M1 (0.5903 g, yield 94%). 1H NMR ($CDCl_3$, ppm): δ 9.18 (d, J = 5.5 Hz, 1H, H_E), 8.42 (d, J = 2.4 Hz, 1H, H_A), 8.15 (d, J = 8.1 Hz, 1H, H_F), 8.01 (t, J = 7.1 Hz, 1H, H_G), 7.47 (dd, J = 8.6, 2.4 Hz, 1H, H_C), 7.03 (d, J = 6.5 Hz, 1H, H_D), 6.01 (d, J = 8.6 Hz, 1H, H_B).

2.2.2 Synthesis of [Ir(ppy)2](OTF)2 (M2)

Compound M1 (0.1225 g, 0.1mmol) in 5 mL of dry 1-ethoxy-2-(2-ethoxyethoxy) ethane was heated to dissolve all of the chloro-bridged dimer. A 3 mL 1-ethoxy-2-(2-ethoxyethoxy) ethane solution of AgOTf (0.054g, 0.21 mmol) was added to the solution. The mixture was kept at 75°C in the dark for 12h resulted in a gray precipitate. The gray AgCl precipitate was filtered and resulted a yellow solution. The solution was concentrated in vacuo, then redissolved in a minimal amount of tetrahydrofuran and precipitating with diethyl ether. The yellow crystal precipitate were collected and dried under vacuum to give the product M2 (0.1602 g, yield 89%).

2.2.3 Synthesis of fac-Ir-NO2

Compound M_2 (0.13 g, 0.15 mmol) and L_1 (0.06 g, 0.3 mmol) were combined in 15 mL of 1-ethoxy-2-(2-ethoxyethoxy) ethane and heated at 160 °C under N_2 atmosphere for 100 h. After cooling to room temperature, the reaction solution was chromatographed on a silica gel column packed with petroleum ether to first elute o-dichlorobenzene. The solution was concentrated in vacuo, then redissolved in a minimal amount of acetonitrile and precipitating with diethyl ether. The yellow crystal precipitate were collected and dried under vacuum to give the product ***fac*-Ir-NO$_2$** (0.08 g, yield 67%). 1H NMR ($CDCl_3$, ppm): δ 8.54 (d, J = 2.4 Hz, 1H, H_E), 8.11 (d, J = 8.2 Hz, 1H, H_A), 7.84 (td, J = 7.8, 1.6 Hz, 1H, H_F), 7.67 (dd, J = 8.4Hz, 1H, H_G), 7.52 (d, J = 5.5 Hz, 1H, H_C), 7.15 – 7.08 (m, 1H, H_D), 6.90 (d, J = 8.4 Hz, 1H, H_B).

2.2.4 Synthesis of fac-Ir-NH2

The catalyst Pd/C(10%) and hydrazine hydrate (80%, 15 equiv) were used for reduction ***fac*-Ir-NO$_2$** to ***fac*-Ir-NH$_2$**, and ethanol was chosen as the solvent (90% yield). 1H NMR (DMSO-d_6, ppm): δ 7.837 (d, J = 6.0 Hz, 1H, H_E), 7.741 (t, 1H, J = 6.0 Hz, H_A), 7.435 (d, J = 3.9 Hz, 1H, H_F), 7.052 (m, 2H, H_G,H_D), 6.407(d, J = 6.0 Hz, 1H, H_B), 4.839 (m, 2H, H_H).

2.2.5 Synthesis of fac-Ir^(C=N)3

To a Schlenk tube was added ***fac*-Ir-NH$_2$** (0.07g, 0.1 mmol, 1equiv.), 2-formylpyridine (0.063g, 0.6 mmol, 6 equiv.) in ethanol (10 mL). The solution was refluxed for 24 h under the protection of N_2. Then the solution was placed in a sealed tank full of N_2 and diffused with diethyl ether then the dark yellow solid was obtained (yield 90%). 1H NMR (DMSO-d_6, ppm): δ 8.817 (d, J = 3.3 Hz, 1H, H_5), 8.68 (s, 1H, H_1)8.379 (m, 1H, H_A), 8.15 (d, J = 8.4 Hz, 1H, H_E), 7.93 (d, J = 17.0 Hz, 3H,H_4,H_3,H_G), 7.52 (d, J = 32.0 Hz, 2H, H_2, H_C), 7.23 (s, 1H,H_D), 6.82 (d, J = 8.4 Hz, 1H, H_F), 6.798 (d, J = 6.0Hz, 1H, H_B).

2.2.6 Synthesis of Ir-Zn

To a Schlenk tube was added *fac*-Ir^(C=N)$_3$ (58 mg, 0.06 mmol, 1.5 equiv.), Zn(OTF)$_2$ (14.5 mg, 0.04 mmol, 1 equiv.) in acetonitrile (10 mL). The solution was refluxed for 24 h under the protection of N_2. (yield 92%).

3. Result and discussion

3.1 Spectral characterization

Compound Ir–Zn was obtained by the reaction of fac-tris(5-(2-pyridinyl) phenylamine) iridium and 2-formyl pyridine via a subcomponent self-assembly in the presence of Zn(OTF)$_2$ using acetonitrile as solvent. Diffusing diethyl ether into the above-mentioned solution gave a solid compound Ir–Zn in 92% yield. Fig.1 shows Ir-Zn's morphology and energy-dispersive spectrum

(EDS) mapping. The 4 elements are evenly distributed in the sample, Fig.1 proves that the synthesized sample is uniform and stable.

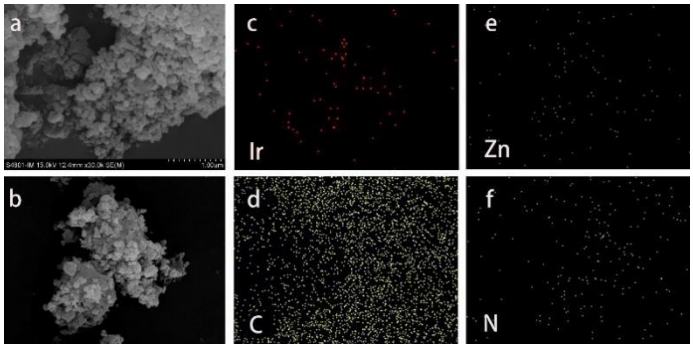

Fig. 1. (a) SEM image of Ir-Zn(1μm). (b) SEM image of Ir-Zn(600μm). (c) Element-mapping image of Ir. (d) Element-mapping images of C. (e) Element-mapping images of Zn. (f) Element-mapping images of N.

The functional bonds of the Ir-Zn are shown in Fig.4. The absorption band at 1634 cm^{-1} respectively attributed to the stretching and bending vibration of C=N. The peaks at 1425 cm^{-1} 1470 cm^{-1} 1566 cm^{-1} and 1600 cm^{-1} belong to characteristic absorptions of the benzene.

Fig.2 shows UV−vis absorption spectra of Ir^$(C=N)_3$(black) and Ir-Zn(red). Ir-Zn has a strong UV absorption band at 240 nm and 280 nm (Fig. 2), which is associated with the existence of bpy (bpy=Benzopyridine) groups. After adding Zn(II), Ir-Zn exhibits more excellent UV absorption ability as shown in Fig. 2. Besides, the peak at 390 nm disappeared, and a new peak appeared at about 430 nm, which could be classified as a p-p* transition, which is to ligand-to-metal charge transfer (LMCT). It showed that the coordination of Zn^{2+} with the binding site of the C=N bond leads to the change in UV–Vis spectrum.

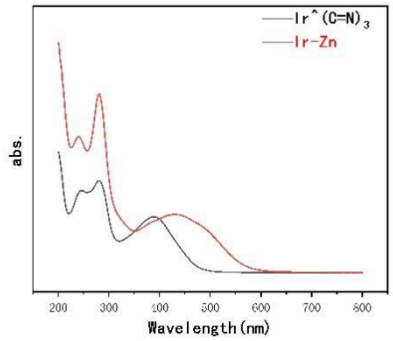

Fig 2. UV−vis absorption spectra of Ir^$(C=N)_3$(black) and Ir-Zn(red).

Fig. 3 presents the spectra of the sample and shows that the sample is uniform and stable. Ir(III) has not changed. By curve fitting the Zn 2p1/2 XPS spectra, Fig. 3 shows that two Zn species were discriminated in the Ir-Zn, the N1s spectra of the sample. After interaction of Zn (II) with the Ir^$(C=N)_3$, the N1s peak shifts to lower energies (ΔE = 2.4 eV) and is observed at 399.18 eV, indicating Ir^$(C=N)_3$ interact with Zn (II).

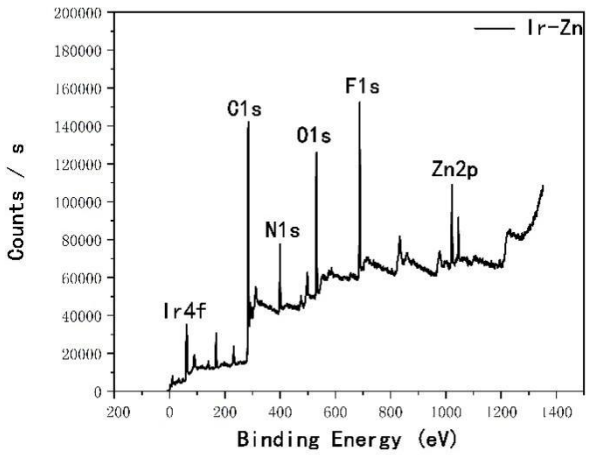

Fig 3. XPS survey spectrum of Ir-Zn.

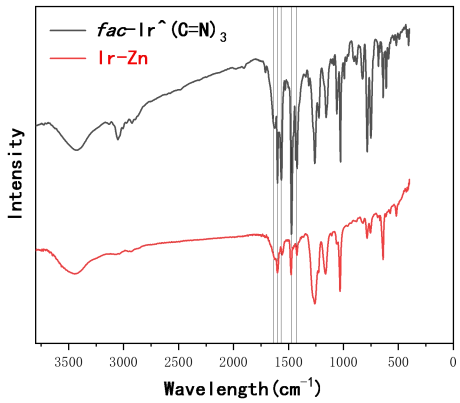

Fig.4. FT-IR of *fac*-Ir^(C=N)$_3$ (black) and Ir-Zn (red).

3.2 CO_2 Reduction

The photocatalytic reduction of CO_2 was conducted using Ir-Zn. Specifically, a DMA/TEOA solution (5:1 v/v) containing 0.05 mM of Ir-Zn was irradiated under a 300W Xe lamp under a CO_2 atmosphere, and selectively afforded CO (Fig 6). Especially after irradiation for 1 h, the CO formation continuously increased over time, while its turnover number (TONCO), which was calculated as [product (mol)]/ [added Ir-Zn (mol)], was 176 and the CO selectivity (SCO) was >99%. After 6 h of irradiation, TONCO reached 312. Fig.4 shows that the Ir-Zn polymer has great long-term cycling performance, after 90 cycles the sample maintains 98.5% (307.5/312) activity. The decrease in CO_2 reduction capacity may be related to the partial decomposition of the sample, although the compounds reported in this paper have good stability at room temperature and light, the xenon lamp we use emits a lot of heat when illuminated, which increases the temperature of the entire reaction system. Therefore, it may cause some damage to the catalyst, but this has little effect on the effect of CO_2 reduction. Fig.8 shows that when *fac*-Ir^(C=N)$_3$ is over-doubled, TONCO has a weak boost. This is due to the excessive photocatalyst, the electron transport capacity is enhanced, but the catalytic site in the product is certain, so the reaction rate is limited. Since the binding site of photosensitizer and catalyst is fixed, increasing the concentration of zinc ions does

not affect the catalytic effect. When zinc ions are not added, the effect of CO_2 reduction by the photosensitizer itself is poor. When only $Zn(OTF)_2$ is added, CO_2 reduction cannot be catalyzed because there is no photosensitizer to provide photogenerated electrons under light. In summary, *fac*-Ir^(C=N)$_3$: $Zn(OTF)_2$ =3: 2 is the best feeding ratio.

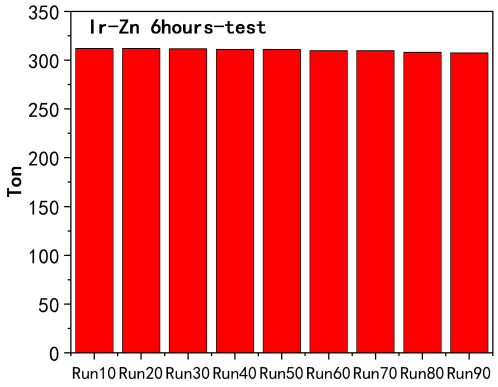

Fig 5. Catalytical cyclic tests of Ir-Zn

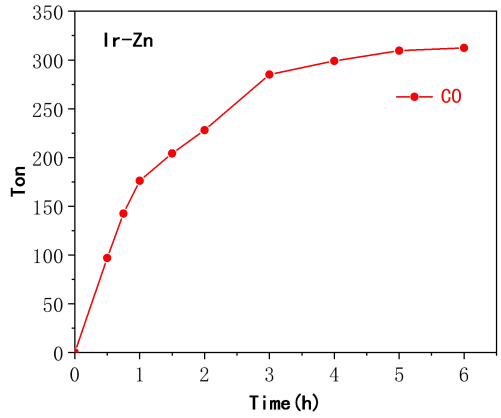

Fig 6. Time courses of CO (red) formation in the initial stage of the photocatalytic reaction using a DMA/TEOA solution (5:1 v/v) containing 0.05 mM of Ir-Zn.

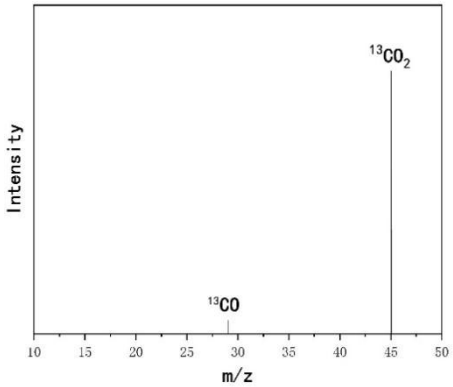

Fig 7. Gas chromatogram and mass spectra (GC–MS) analysis for solardriven reduction of $^{13}CO_2$ to ^{13}CO (m/z = 29) with Ir-Zn as photocatalyst.

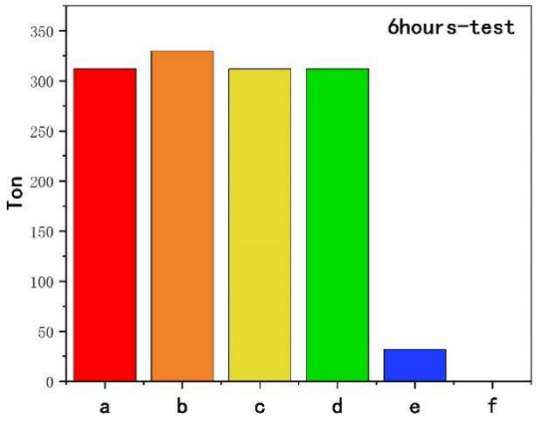

Fig 8. Differential ton (CO) of DMA-TEOA (5:1 v/v) solutions containing the complex (0.5 mM). (a) *fac*-Ir^(C=N)$_3$: Zn^{2+} = 1.5:1. (b) *fac*-Ir^(C=N)$_3$: Zn^{2+} = 3:1. (c) *fac*-Ir^(C=N)$_3$: Zn^{2+} = 1:1.5. (d) *fac*-Ir^(C=N)$_3$: Zn^{2+} = 1:3. (e) *fac*-Ir^(C=N)$_3$. (f) Zn (OTF)$_2$. All sample were exposed to 300w xenon light for 6 hours.

At the same time, to further clarify good CO selectivity for the photocatalytic CO_2 reduction over Ir-Zn, the Agilent 7890A/5975C Gas chromatogram and mass spectra (GC–MS) is employed to analyze the products of $^{13}CO_2$ isotopic experiment and to determine whether other potential C-based products are generated. $^{13}CO_2$ is used for the photocatalytic reaction under the same reaction conditions. The products from the isotopic experiment are analyzed by GC–MS, and the results are displayed in Fig. 7. It can be found that there exists the appearance of $^{13}CO_2$ to ^{13}CO (m/z = 29). Meanwhile, no other products were observed by the GC–MS. This provides powerful proof that Ir-Zn exhibits good CO selectivity and CO originated from the deoxygenated conversion of CO. Table 1 shows that the compounds prepared in this paper show a higher conversion rate and excellent selectivity compared with previously reported photocatalysts.

Table 1 photocatalysts for CO_2 reduction.

Photocatalyst	Light	Product	Yield	Ref.
Bi_2MoO_6	visible light	CO	3.62 μmol. $g^{-1}.h^{-1}$	28
Bi_2MoO_6	visible light	CO	2.01 μmol. $g^{-1}.h^{-1}$	29
Bi_2MoO_6	300 W Xe lamp	CO	17.104 μmol. $g^{-1}.h^{-1}$	30
Au/g-C_3N_4	300 W Xe lamp	CO	28.3 μmol. $g^{-1}.h^{-1}$	31
AuCu/TiO_2/ZIF-8	AM1.5 Xe lamp	CO	80 μmol. $g^{-1}.h^{-1}$	32
Au-TiO_2 (101)	UV cutoff filter 320<λ<420 nm; 33 $mWcm^{-2}$	CO	25.9 μmol. $g^{-1}.h^{-1}$	33
Ir-Zn	300 W Xe lamp	CO	4366 μmol. $g^{-1}.h^{-1}$	

4. Conclusion

In conclusion, via the incorporation of a fac-tris(5-(2-pyridinyl)-phenylamine) iridium as the backbone of the tripodal ligand, a metal-organic polymer Ir–Zn was obtained via subcomponent

self-assembly. The Zn (II) ions in the structure induced atmospheric carbon dioxide transformation to the metal centers. The predesigned conformation of the Ir-Zn precursor benefits the precise control of the polymer geometry. Work is currently in progress on further modification of the Ir-Zn precursor, providing the possibility of tuning the metal atom center and organic ligands bonding behavior toward other reactive substrates. In addition, we also hope to further study the catalytic effect of heterogeneous photocatalytic systems in the future. The preparation of compounds by pre-designed structures has become one of the research hotspots, and the use of special coordination structures of precious metals can further improve the success rate of metal-organic compound preparation, thereby greatly shortening the experimental time. Therefore, the combination of precious metals and transition metals to prepare metal-organic compounds has very interesting research prospects.

Acknowledgments

The authors are very grateful to MOE Key Laboratory of Cluster Science, Beijing Key Laboratory of Photoelectronic/Electrophotonic Conversion Materials, School of Chemistry and Chemical Engineering, Beijing Institute of Technology for their support.

Reference

[1] G.A. Olah, G.K. Prakash, A. Goeppert, J. Am. Chem. Soc. 133 (2011) 12881–12898.

[2] M. Aresta, A. Dibenedetto, A. Angelini, Chem. Rev. 114 (2014) 1709–1742.

[3] A.J. Morris, G.J. Meyer, E. Fujita, Acc. Chem. Res. 42 (2009) 1983–1994.

[4] S.S. Mao, S. Shen, Nat. Photonics 7 (2013) 944–946.

[5] X. Feng, Y. Pi, Y. Song, C. Brzezinski, Z. Xu, Z. Li, W. Lin, J. Am. Chem. Soc. 142 (2020) 690–695.

[6] X.Y. Dao, X.F. Xie, J.H. Guo, X.Y. Zhang, Y.S. Kang, W.Y. Sun, ACS Appl. Energy Mater. 3 (2020) 3946–3954.

[7] X. Chang et al., Energy Environ. Sci. 9 (2016) 2177–2196.

[8] W. Tu et al., Adv. Mater. 26 (2014) 4607–4626.

[9] K. Li et al., ACS Catal. 6 (2016) 7485–7527.

[10] S. Hennessey, P. Farras, Chem. Commun. 54 (2018) 6662–6680.

[11] J. Kou et al., Chem. Rev. 117 (2017) 1445–1514.

[12] O. Ola, M.M. Maroto-Valer, J. Photochem. Photobiol. C 24 (2015) 16–42.

[13] Y. Zhao et al., Chem. Soc. Rev. 48 (2019) 1972–2010.

[14] C. J. Brown, F. D. Toste, R. G. Bergman, K. N. Raymond, Chem. Rev. 115 (2015) 3012 – 3035.

[15] M. Yoshizawa,J. K. Klosterman, M. Fujita, Angew. Chem. Int. Ed. 48 (2009) 3418 – 3438.

[16] M. Yoshizawa,J. K. Klosterman, M. Fujita, Angew. Chem. 121 (2009) 3470 – 3490.

[17] M. Raynal,P. Ballester, A. Vidal-Ferran, P. W. van Leeuwen, Chem. Soc.Rev. 43 (2014) 1734 – 1787;

[18] T. R. Cook, P. J. Stang, Chem. Rev. 115 (2015) 7001 – 7045.

[19] Y. Kohyama, T. Murase, M. Fujita, Angew. Chem. Int. Ed. 53 (2014) 11510 – 11513;

[20] Y. Kohyama, T. Murase, M. Fujita, Angew. Chem. 126 (2014) 11694 – 11697;

[21] T. Murase, Y. Nishijima, M. Fujita, J. Am. Chem. Soc. 134 (2012) 162 – 164;

[22] D. M. Kaphan, F. D. Toste, R. G. Bergman,K. N. Raymond, J. Am. Chem. Soc. 137 (2015) 9202 – 9205;

[23] D. M. Dalton, S. R. Ellis, E. M. Nichols, R. A. Mathies, F. D.Toste, R. G. Bergman, K. N. Raymond, J. Am. Chem. Soc. 137 (2015) 10128 – 10131;

[24] S. Mukherjee, P. S. Mukherjee, Chem.Commun. 50 (2014) 2239 – 2248;

[25] Holloway, S.; Pearce, J.; Hards, V.; Ohsumi, T.; Gale, J. Energy. 32 (2007) 1194−1201.

[26] Zhang, J., Yagi, M. and Kaneko, M. Macromol Symp, 105 (1996) 59-66.

[27] Yagi M, Kinoshita K, Kaneko M. The Journal of Physical Chemistry, 100(1996): 11098-11100.

[28] J. Di, X. Zhao, C. Lian, M. Ji, J. Xia, J. Xiong,W. Zhou, X. Cao, Y. She, H. Liu, K.P. Loh, S.J. Pennycook, H. Li, Z. Liu, Nano Energy 61 (2019) 54–59.

[29] X. Yang, S. Wang, N. Yang, W. Zhou, P. Wang, K. Jiang, S. Li, H. Song, X. Ding, H. Chen, J. Ye, Appl. Catal. B Environ. 259 (2019) 118088

[30] L. Cheng, L. Liu, D. Wang, F. Yang, J. Ye, J. CO2 Util. 29 (2019) 196–204

[31] F. Li, H. Zhou, J. Fan, Q. Xiang, J. Colloid Interface Sci. 2020, 570, 11–19.

[32] T. Butburee, Z. Sun, A. Centeno, F. Xie, Z. Zhao, D. Wu, P. Peerakiatkhajohn, S. Thaweesak, H. Wang, L. Wang, Nano Energy 2019, 62, 426–433.

[33] A. Wang, S. Wu, J. Dong, R. Wang, J. Wang, J. Zhang, S. Zhong, S. Bai, Chem. Eng. J. 2021, 404, 127145.